RSC Advances

ROYAL SOCIETY OF CHEMISTRY

www.rsc.org/advances

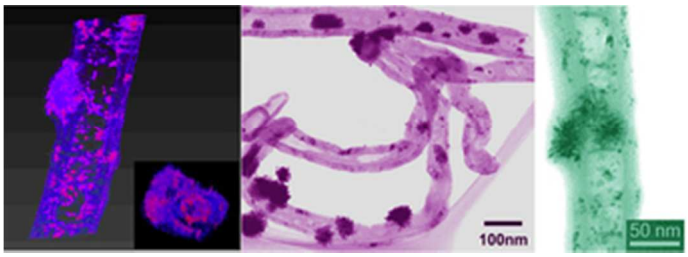

Novel catalysts with Pt nanorod clusters distributed in both interior and exterior of CNTs were prepared and confirmed by TEM tomography. This structure benefits higher performance due to the CNTs' confinement effect.
28x10mm (300 x 300 DPI)

Enhancement of the catalytic performance of CNT supported Pt nanorod cluster catalyst by controlling their microstructure

Cuifeng Zhou[1], Xusheng Du[2*], Hongwei Liu[3], Simon P. Ringer[2, 3], Zongwen Liu[1*]

[1] School of Chemical and biomolecular engineering, The University of Sydney, NSW 2006, Australia

[2] Centre for Advanced Materials Technology, School of Aerospace Mechanical & Mechatronic Engineering J07, The University of Sydney, NSW 2006, Australia

[3] Australian Centre for Microscopy and Microanalysis, The University of Sydney, NSW 2006, Australia

Abstract: Novel Pt/CNT catalyst with hierarchical structure was prepared. The effect of different morphology of CNT supports on the catalyst microstructure and catalytic performance was studied. TEM tomography was used to analyse the real microstructure of the catalysts, including both the morphology of flower-like Pt clusters themselves and their distribution on the CNTs. The results revealed that Pt flowers were composed of nanorods, which dispersed in both the inner and outer tube surface of CNTs with larger inner tube diameter (TKCNTs). Comparing with the conventional Pt/CNT catalyst where Pt flowers only dispersed on the outer tube surface, the present Pt/TKCNT catalyst with the novel structure exhibited higher activity (enhanced to be ~1.5 times higher current density) and better catalytic stability for methanol oxidation. Moreover, it displays ~2 times higher activity for methanol electro-oxidation than that of CB supported Pt nanorod clusters. The results indicate that the catalytic performance of the Pt nanorods supported on different carbon supports depends on both carbon morphology and the distribution of metal catalyst on the supports. The improved catalytic performance of Pt/TKCNT catalyst with the novel hierarchical structure could be attributed to the confinement effect of TKCNTs.

*Corresponding author: Fax: +61-2-9351-7682; E-mail:xdu@usyd.edu.au(XDu); zongwen.liu@sydney.edu.au(ZLiu)

1 INTRODUCTION

The electrochemical reaction in the electrolyte is usually a process carrying out at the interface and therefore the topography of the catalyst has great influence on catalytic performance. However, the microstructure characterization of the samples is not straightforward with respect to the multi-dimensional catalyst particles (or clusters) and their distribution on the catalyst supports. TEM tomography appeared to be a very suitable technique for such characterization. It was demonstrated to be a good method to examine the real dispersion of metal particles in the porous supports, including CNTs and other mesoporous materials [1-3], which is always improper interpreted by the conventional 2D TEM images. Moreover, it was successfully used to characterize complex Pt nanostructures recently [4-6]. As the catalytic performance is dependent on the whole catalyst topography structure, the disclosure of the real morphology of active catalyst particles and their distribution on supports is important to further design and development of high efficient catalysts.

Platinum (Pt) based catalysts has been widely utilized in industries, such as the reduction of pollutant gases emitted from automobiles, oil cracking, and fuel cells[7]. The direct methanol fuel cell is a green power source, where Pt catalysts were used both to oxidize methanol fuel at the anode[8-10] and to reduce oxygen from air at the cathode to produce electricity [11]. In order to improve catalyst performance, durability and utilization as well as to lower the cost of fuel cells, supported catalysts are preferred to be used. Hence, improvement and optimization of an electrocatalyst could be achieved in the aspects of Pt catalyst, and the supporting materials including the dispersion of Pt on the supporting materials. Catalytic performance of Pt nano-materials can be adjusted through the control of their structure, including their crystal structure, shape and size [12-29]. Various Pt nanostructures (such as nanowires, nanotubes, nanodendrites, nanoflowers) have been reported. Most of these unique morphologies, especially those based on 1D Pt nanostructures grown along (111) crystal plane, display excellent electrochemical catalytic activity[13-29].

On the other hand, the supporting materials of catalysts also have great impact on the electrochemical performance of the catalysts. Various materials have been studied as supports for Pt-based electrochemical catalysts [30], including conductive polymers [31-39], and various carbon nanomaterials [13, 40-55]. The commercial Pt is usually supported on carbon black. Compared to the widely used carbon black, CNTs are attracting more and more interest due to their structural tube features, low resistance and high stability in electrochemical reactions. The hollow interior of CNTs provides a nanoreactor for the electrochemical reactions. The interactions (including electron transfer) between confined nanomaterials and carbon walls are believed to be different from those happened on the nanomaterials on outer tube surface. These benefit the higher catalytic performance due to the confinement effect of CNTs [56-58]. The spatial confinement of bimetallic PtRu NPs in CNTs have also demonstrated to benefit their catalytic performance for the selective hydrogenation of cinnamaldehyde [56]. Besides of CNTs, other supporting materials with similar tube structure (such as copper phyllosilicate nanotube) also displayed positive effect on the catalytic performance [59]. However, the information on the structure and performance of catalysts with the combination of the 1D Pt nanostructure and the confinement effect of CNTs was less explored so far.

Here, a novel catalyst with Pt nano-materials supported on thick carbon nanotubes with large inner tube space (TKCNTs) was reported. In the catalyst, Pt nanorod clusters dispersed on both interior and exterior of TKCNTs. According to the aforementioned discussion, it is expected that Pt/TKCNTs with such a unique structure will show enhanced catalytic activity. Previous study in the area always focused on the different type of catalyst supports or the morphology of catalyst particles. However, the distribution of metal catalyst and the confinement effect of CNTs have less been explored, although they also have great influence on their catalytic performance and applications [56-58]. Therefore, further discussion of Pt catalyst performance controlled by the topography structure of the catalyst is of great interest and importance. For reference, we also prepared the

Pt/CNT catalyst with the common structure where Pt nanorod clusters only dispersed on the outer tube surface. As a demonstration of the effect of catalyst structure on the properties, their electrochemical catalysis on methanol oxidation was studied and compared.

2 EXPERIMENTAL

2.1 *Materials*

Vulcan XC-72 carbon black (CB) was obtained from Cabot Company. The thick carbon nanotube (Pyrograf Products Inc., named 'TKCNT' here) with outer diameter of 50 – 150 nm was first treated with a conventional chemical oxidation method using concentrated nitric acid to remove the metal impurities. Multi-walled carbon nanotubes (named 'TNCNTs' here) with outer diameter of 30 – 50 nm were purchased from Chengdu Organic Chemicals Co., Ltd. Their surfaces were pre-functionalized with the carboxylic acid functional groups (-COOH) and used as received.

2.2 Nanocatalyst fabrication and the methanol oxidation

Pt particles dispersion on the catalyst supports were prepared by a method of *in situ* reduction of a Pt salt with formic acid. 0.2 g $H_2PtCl_6 \cdot H_2O$ was dissolved in 10 ml distilled water. The catalyst support TKCNTs were dispersed in distilled water by sonication for 20 min. Then, an appropriate amount of $H_2PtCl_6 \cdot H_2O$ solution was added dropwise to the above support suspension with sonication. After adding formic acid, the suspension was stored at room temperature for 4 days to complete the reduction of Pt. After centrifugation and washing with water and ethanol, the material was dispersed in 0.05 wt% Nafion solution and sonicated for 20 mins to prepare the catalyst ink. 3.5 μL of this catalyst solution was added to the surface of the glassy carbon (GC) electrode (3 mm in diameter) and dried in air. For comparison, the catalyst with CB and TNCNT as supports was also

prepared under the same experimental conditions, respectively. Energy Dispersive Spectroscopy analysis indicated that the Pt content in all catalysts was ~55 wt%. Prior to the electrochemical measurement, the catalyst covered electrode was soaked in the electrolyte solution (0.5 M H_2SO_4) for 10 min. The electrochemical activity of the catalyst with respect to methanol oxidation was tested in 1M CH_3OH+0.5M H_2SO_4.

2.3 Characterization and Measurements

X-ray diffraction (XRD) patterns were obtained using an X-ray diffractometer (Siemens D5000) with Ni-filtered Cu Kα radiation (λ=1.54 Å). Scanning electron microscopy (SEM; Zeiss ULTRA plus) was used to observe the morphology of the samples. Transmission electron microscopy (TEM) was on the following instruments: routine imaging - Philips CM12 (120 kV), high resolution TEM (HRTEM) and EDS microanalysis - JEOL 2200FS (200 kV); electron tomography-JEOL 1400 (120kV). The 2D experimental images for 3D-TEM (electron tomography) were recorded in a bright-field mode on a JEOL 1400 (120 kV) using a high-tilt sample holder. The tilt series were acquired with automatic rectification (corrections of focus and horizontal displacement) by using the Serial EM[60] software on a 1350×1040 pixel Erlangshen CCD camera (Gatan). The tilt range was set from -75° to 65°, with a basic increment of 1°, giving a total of 140 images. The tilt series data were treated for image processing and reconstruction using the composer and visualization softwares program. The electrochemical characterisations were performed on a CHI1202A Electrochemical Analyzer (CH Instruments). All the solutions were prepared in distilled water and all potentials reported were referenced to a saturated calomel electrode (SCE). A three-electrode electrochemical cell was used for the measurements, where the counter electrode was a Pt foil and the reference electrode was a SCE.

3 RESULTS AND DISCUSSION

In the XRD patterns of TKCNT/Pt (Fig.1a), four peaks around 2θ = 40.1º (111), 46.4º (200), 68.1º (220) and 81.5º (311) are observed, which are contributed from Pt. The peak centered at 26.3º is typically from (002) of CNTs. Figure 1b and 1c shows the morphologies of the TKCNT/ Pt catalysts. In SEM image (Figure 1b), the white grains and clusters on the TKCNT surface are Pt nanocatalysts, but they are displayed as the black clusters and grains in the TEM image (Figure 1c). Correspondingly, the inner diameter of TKCNTs can be up to 20-100nm, which provides enough space for the convenient in situ deposit of metal nanoparticles or further chemical reaction for the nanocatalyst in the inner tube. HRTEM image confirms that the flowers are indeed composed of Pt nanorods with diameter in the range of 2-5 nm (Figure 1d), and the crystallographic alignment of these nanorods reveals that all nanorods are one single crystal. A lattice spacing of 0.223 nm in the longitude direction of the rods can be clearly observed, indicating that the Pt nanorods grow along the (111) direction. The selected-area electron diffraction (SAED) pattern (inset in Figure 1c) displays several concentric rings assignable to (111), (200), (220), and (311) crystal planes, indicating that the obtained Pt rods are crystallized in a face-centered cubic (FCC) phase, which is consistent with the XRD result (Figure 1a).

Generally, this anisotropic growth of 1D Pt nanocrystals is always attributed to the slow reduction rate and the lowest energy principle. A few reports are available on the direct growth of Pt nanowires, or flowers on the surface of conductive carbon and carbon nanotubes using HCOOH as a slow reducing agent[11,18,51-52]. Recently, the synthesis of Pt flowers on the outer surface of CNTs using L-ascorbic acid as reducing agent was achieved with a polymer (chitosan or PSS) wrapping method [55]. In our fabrication process, no surfactant and template was used, thus make the approach simple and avoid of the possibility of any catalytically harmful structure-directing moieties. To understand the present growth mechanism of Pt nanoflowers, samples at different time intervals (4, 12, 36 and 72 h) was collected and performed the TEM analysis. Interestingly, the sample collected after 4h of

reaction shows the presence of Pt nanoparticles with a diameter of 2-5nm distributed on the TKCNTs (Figure 2a). This observation suggests that the reduction of Pt ions already takes place and the resulted nanoparticles in situ attached on the TKCNT surface. After the reaction of 12h, almost all TKCNTs were deposited with Pt particles and some Pt clusters started to appear, however no nanorod was observed (Figure 2b). After the reaction of 36h, Pt nanorods are formed on the TKCNT surface (Figure 2c), and the diameter of the nanorods is in the same range as that of Pt nanoparticles formed at 12h of reaction (see Figure S1 in $^{+}$ESI), indicating of the 1D growth of Pt nanorods along the (111) direction (Figure 1d), and a few Pt flowers composed of nanorods can be also observed. After 72h of reduction, the morphology of Pt clusters (Figure 1c) did not change too much compared with the ones collected at 36h. With the aforementioned TEM and XRD data, we can conclude that the Pt nanoparticles are forming first by the reduction of the Pt ions in the initial stage. These nanoparticles deposited on the surface of the TKCNTs acts as seeds for further growth of the nanostructure along (111) crystal plane through the further adsorption and reduction of Pt ions. This facilitates the further growth of the Pt nanorods and self assembly into flower-like clusters.

Pt nanowires, dendrite, flower-like and other hierarchical nanostructures are promising catalysts due to their high surface area and high-index crystal facets, which provide lots of active corner and edge sites. The presence of the CNTs as supports is expected to further improve the utilization and distribution of the Pt catalysts, and thereafter help to improve their electrochemical catalytic performance. Figure 3a illustrates the electrochemical catalytic activity of the carbon material supported catalysts towards oxidation of methanol in acidic solution, in which the forward current peak is attributed to the oxidation of CH_3OH molecule and the backward current peak to the oxidation of the adsorbed intermediates [35-36]. Obviously, the methanol oxidation current intensity on both TKCNT and TNCNT supported Pt catalyst is much larger than that on CB/Pt, and the forward peak current density on TKCNT/Pt is more than 2 times of that on CB/Pt, indicating the beneficial effects of CNT supports

over the conventional CB supports. Furthermore, the catalytic performance of TKCNT/Pt catalyst is much better than that on TNCNT/Pt catalyst, as both of the peak current intensity on the TKCNT/Pt catalyst is larger than that on TNCNT/ Pt catalyst and the forward peak current density on TKCNT/Pt is more than 1.5 times of that on TNCNT/Pt.

The stability of the electrochemical catalytic activity is one of the important properties of a catalyst. To compare this performance of three catalysts, we conducted chronoamperometry tests. Figure 3b shows the chronoamperograms for the oxidation of methanol on the TKCNT/Pt and TKCNT/Pt catalysts in acidic media. The current density shows sharp decay in activity on both catalysts in the first 20 s, which could be related to the adsorbed intermediate products of methanol oxidation on the surface of the fresh Pt catalysts, such as CO_{ads}, $COOH_{ads}$, and CHO_{ads}, during the methanol oxidation reaction. After that, the current density generally reaches a steady state. The current density gradually decreases with time because methanol is electrochemically oxidized continuously and the concentration of methanol decreases with time, and the current can also be attributed to the accumulation of CO_{ads} poison species on the surface of Pt nanocatalysts during the process of the methanol oxidation. The slower decay of steady-state current indicates that the catalyst has high tolerance toward poisoning by CO-like intermediates. The current density on TKCNT/Pt catalyst is much higher than that of TNCNT/Pt catalyst throughout the whole chronoamperograms test, and both of them are larger than that of CB/Pt. Interestingly, in the nearly steady state, for instance, the current density of methanol oxidation at 400 s on the TKCNT/Pt catalyst is ~13 times of that on the TNCNT/Pt (Figure 3b). Moreover, in the CV curves measured just after the 900s chronoamperograms tests of the catalysts, the forward peak current density for the methanol oxidation on the TKCNT/Pt decreased only 15%, which is much less than those on TNCNT/Pt (~50%), as shown in Figure 3c and 3a. The higher stability of the catalytic current intensity on the catalyst with TKCNT support than that with TNCNT is believed to be related to the microstructure of the catalyst, and

it is worthwhile to investigate further to reveal the effect of different carbon supports on the performance of the catalysts. Recently, the pronounced impact of the three-dimensional nano-spatial distribution of metal catalyst particles on catalyst stability was also demonstrated, indicating the importance of the distribution of the catalysts on the supports [2,59].

The morphology of the Pt cluster supported on the TNCNTs and CB were shown as Figure 4a-c and d, respectively. Different to the morphology in Pt/TKCNTs, the flower-like Pt clusters on the TNCNTs were only dispersed on the outer tube surface, similar to the other results [53]. This is because the inner tube diameter of the TNCNTs (most of them less than 10nm) is too small to afford enough space for the in situ deposition of flower-like Pt nanorod clusters. HRTEM of the TNCNT/Pt show that the Pt flowers are also composed of nanorods growing along (111) directions (Figure 4c). As the Pt clusters in the TKCNT/Pt and TNCNT/Pt have similar structure, the enhancement of the electrochemical catalytic performance of TKCNT/Pt should be due to the different catalyst support and the distribution of the metal catalyst nanoparticles on the support.

Conventional TEM image is a 2D projection of a 3D structure, which is difficult to provide 3D information conveniently with a single TEM image and sometimes give misleading results [1, 4]. For example, in a normal TEM image, the location of particles in area A cannot be determine surely as those in area B in Figure 5a. And the relative nano-spacial distribution of the three particles on a tube (two particles in the inside and one outside the tube) in Figure 5a is difficult to locate due to the 2D projection image obtained by transmission electron is likely as Figure 5b. Although STEM technique may be possible to locate the particles on the outer surface of the tube due to the outstanding contrast of inner tube in the image (as shown Figure 5c and d), it remains to be a great challenge to determine whether the particles are in or out side of the tube when they are distributed in area A in Figure 5a.

In order to study the exact 3D microstructure of objects, TEM electron tomography (also named '3D TEM') was thus developed. Such a 3D structure representation was reconstructed from a tilt series of 2D projection images [1-6]. It is a very suitable technique that can clearly determine the exact location of the catalyst particles with respect to tube-like nanomaterials [51, 1-3]. TEM images taken during rotation of one tube about its axis can provide detailed information on the locations and shape of the Pt nanocatalysts inside/outside the tube by following the movement. Selected TEM tilt images of TKCNT/Pt show the same area but with different perspectives with tilting the sample from +50° to -72° (Figure 6). Clearly, some particles inside the tube (for instance, the highlighted ones in a blue circle) move steadily around the tube axis as the tube is tilted continuously within the inner tube; while the particles (the highlighted ones in a red circle) that appear initially to be located in the inner tube at $+50^{o}$ move progressively toward the outer wall ($+30^{o}$), reach it at 0^{o} and cross it at -30^{o}. In contrast, no Pt particle was observed to be located in the inner tube of TNCNTs, as illustrated in Figure S2 in $^{+}$ESI. It's found that the diameter of the inner tube of the TNCNT is non-uniform along the tube longitude direction (varied between 1-10nm) and the inner tube wall exhibit river-like 'Zig-Zag' morphology, which is unfavoured for the in situ electrochemical deposit of Pt catalysts in the inner tube.

The tomography technology could also used to study the real morphology of the multi-dimensional particles and complex clusters, including the short nanorods. Previously, rod-like Cu_2S crystals were successfully characterized to be actually nanodisks with a series of tilting TEM [61]. In this work, it seems to be a challenge to determine the morphology of nanorods, especially the length of rods in the flowers with conventional 2D TEM technique, due to the short length of nanorod and the flower like Pt cluster structure supported on the TKCNTs, which have curved outer and inner tube surface. To clearly demonstrate the 3D tomography technology, Pt/TKCNT with a big flower like cluster on the tube was selected for the TEM tomography analysis. In a normal 2D TEM, the Pt rods usually appear shorter, or even close to sphere particles due to their short length

and small diameter. By tilting the samples, it is possible to measure their real length at certain projection angles. The morphology of the length of a single nanorod in the flower in Figure 6 was clearly observed until the sample was tilted at -72^{o}. The length of rods was measured to be as long as 26nm. Moreover, as shown in the image tilted at -30 and -72^{o} in Figure 6, the large Pt clusters on the TKCNT are composed of three clusters of Pt nanorods. From the tilt series of 2D projection images of the sample, the 3D structure representation was reconstructed. A typical image was shown as Figure 7, where small Pt catalysts are observed in both inner and outer tube surface, plus a big Pt nanorods clusters on the outer tube surface. A representative 3D-rendering video for such a structure is provided as the video 1 in $^{+}$ESI. The respective transverse section thereof was obtained from the reconstructed volumes derived from electron tomography (inset in Figure 7). It shows that there are obvious separation between the Pt cluster and TKCNT, indicating the loose structure of the Pt/TKCNT catalyst. Such a hierarchical structure benefits the improvement of mass transfer during the electrochemical reaction process and utilization of the active Pt catalysts.

The accessibility of the inner tube of the TKCNT/Pt catalyst for the methanol and electrolyte should be good, as the in situ chemical deposit of Pt clusters on both sides of TKCNTs take place in a similar acidic aqueous solution. Additionally, the majority of the TKCNTs have an open-ended and large inner tube diameter. The high distribution of active Pt catalyst in the inner tube provides more active sites for the electrochemical catalytic reaction. Moreover, the larger diameter of the inner tube allow the facile transport of the reactant and resulted molecules and ions to and from the catalyst, increasing the access of reactant to the active sites. All these means the interior tube is readily accessible to the electrolyte and fuel. Furthermore, owing to the confinement effect of the TKCNT supports with length up to 100μm, the methanol molecules are trapped to stay relatively longer and thus be oxidized more efficiently on the surface of the Pt catalyst[50, 62-63]. The fluid flow and mass transfer in the nano-scale channels have recently attracted extensive attention [64-66]. Previous

results in the literatures indicated that fluids including water exhibited ultrafast flow rate through CNTs inner tube compared with the conventional fluid flow theory [64-65]. It was found that the mobilities of ions within carbon nanotube membranes could be approximately three times higher than the bulk mobility and the induced electro-osmotic velocities were four orders of magnitude faster than those measured in conventional porous materials [66]. In the case of the electrochemical oxidation of methanol catalysed by the Pt nanocatalysts located in the inner tube of TKCNTs, the methanol diffusion behaviour in the nano-channel of TKCNTs during the electrochemical processing is very complicated and related to many factors, such as the electrical potential, the electro-osmosis, the electrochemical reactions of methanol, functionality and morphology of tube surface, etc. Further investigations of the electrochemical reaction in the nano-channels of CNTs could be a new important issue and is worthwhile to do in the future. In this study, it is believed that the rapid mass transport and more active sites of the TKCNT/Pt may facilitate water dissociation to produce adsorbed OH groups on the catalyst surface that can accelerate the oxidation of the adsorbed CO intermediates, leading to the enhanced poisoning tolerance and stability of the catalyst [50,67].

4 CONCLUSIONS

Pt nanoflowers were deposited onto CNTs with different morphology and carbon black to be the catalysts. TEM tomography was used to characterize the real hierarchical structures. Results show that the flower-like Pt clusters are composed of nanorods with diameter of 2-5nm. For TKCNTs with large inner tube space, the Pt nanocatalyst was distributed through both the interior and exterior tube. Such a unique structure of the catalyst makes the best use of the surface area of the tubes and the confinement effect of carbon nanotubes, leading to the enhanced ~1.5 times catalytic activity over that of the Pt/TNCNTs catalyst with the conventional microstructure (where Pt nanorods only dispersed outer tube surface). And it displays ~2 times higher current

density for methanol electro-oxidation than that of Pt/CB catalyst. TEM tomography was demonstrated to be an effective technique for the study of the distribution and morphology of the complicated catalyst particles and provide important and precise information for the catalyst microstructure.

Acknowledgements

The authors are grateful for access to the characterization facilities in the Australian Microcopy & Microanalysis Research Facility at the Australian Centre for Microscopy and Microanalysis, University of Sydney. Z. L. wishes to thank the Australian Research Council for funding support (DP130104231).

[+]**ESI Available**: A representative 3D-rendering video of Pt/CNTs with the novel hierarchical structure.

Reference:

[1] J.P. Tessonnier, O. Ersen, G. Weinberg, C. Pham-Huu, D.S. Su and R. Schlogl. ACS Nano 2009, 3(8), 2081-2089

[2] G. Prieto, J. Zečević, H. Friedrich, K. P. de Jong and P. E. de Jongh. Nat. Mater. 2013, 12, 34–39.

[3] J. Zečević, Ad M. J. van der Eerden, H. Friedrich, P. E. de Jongh and K. P. de Jong. ACS Nano 2013, 7, 3698–3705

[4] S. Mourdikoudis, M. Chirea, T. Altantzis, I. Pastoriza-Santos, J. Pérez-Juste, F. Silva, S. Bals and L. M. Liz-Marzán. Nanoscale, 2013, 5, 4776–4784

[5] J. Ustarroz, T. Altantzis, J. A. Hammons, A. Hubin, S. Bals and H. Terryn. Chem. Mater. 2014, 26, 2396−2406

[6] S. Deng, M. Kurttepeli, S.Deheryan, D. J.Cott, P. M.Vereecken, J. A.Martens, S.Bals, G. van Tendeloob and C. Detavernier. Nanoscale, 2014, 6, 6939–6944

[7] Z. Peng and H. Yang, Nano Today, 2009, 4, 143

[8] A. A. Melvin, V. S. Joshi, D. C. Poudyal, D. Khushalani and S. K. Haram, ACS Appl. Mater. Interfaces, 2015, 7 (12), 6590–6595

[9] L.-M. Zhang, Z.-B. Wang, J.-J. Zhang, X.-L. Sui, L. Zhao and D.-M. Gu, Carbon 2015, 93, 1050-1058

[10] M. Wang, X. Song, Q. Yang, H. Hua, S. Dai, C. Hu and D. Wei, Journal of Power Sources. 2015, 273, 624-630

[11] S. Du, K. Lin, S. K Malladi, Y. Lu, S. Sun, Q. Xu, R. Steinberger-Wilckens and H. Dong, Sci. Rep. 4, 6439

[12] N. Tian, Z.-Y. Zhou, S.-G. Sun, Y. Ding and L. W. Zhong, Science, 2007, 316, 732–735.

[13] M. U.Sreekuttan, K. P. Vijayamohanan and K.Sreekumar. RSC Adv, 2013, 3, 6913-21

[14] S. M. Alia, G. Zhang, D. Kisailus, D. Li, S. Gu, K. Jensen and Y. Yan, Adv. Funct. Mater., 2010, 20, 3742–3746.

[15] T. Herricks, J. Chen and Y. Xia, Nano Lett., 2004, 4, 2367–2371.

[16] B. Wu, N. Zheng and G. Fu, Chem. Commun., 2011, 47, 1039–1041.

[17] X. Huang, H. Zhang, C. Guo, Z. Zhou and N. Zheng, Angew.Chem., Int. Ed. 2009, 48, 4808–4812.

[18] S. H. Sun, D. Q. Yang, D. Villers, G. X. Zhang, E. Sacher and J. P. Dodelet, Adv. Mater., 2008, 20, 571–574.

[19] S. Sun, G. Zhang, N. Gauquelin, N. Chen, J. Zhou, S. Yang, W. Chen, X. Meng, D. Geng, M. Banis, R. Li, S. Ye, S. Knights, G. Botton and T. Sham, Sci Rep, (2013), 3: 1775

[20] L. Zhuang, W. Wang, F. Hong, S. Yang, H. You, J. Fang and B. Ding. Journal of Solid State Chemistry 2012,191, 239–245

[21] G. Zhang, S. Sun, M. Cai, Y. Zhang, R. Li and X. Sun, Sci Rep, 2013, 3, 526

[22] X. Wang, Y. Sun, J. Hu, Y.-J. Li and E. S. Yeung, RSC Adv. 2015, 18, 13538-13543

[23] M. Cao, D. Wu and R. Cao, ChemCatChem 2014, 6, 26–45

[24] J. Xu, G. Fu, Y. Tang, Y. Zhou, Y. Chen and T. Lu, J. Mater.Chem. 2012, 22, 13585–13590.

[25] Z. Luo, L. Yuwen, B. Bao, J. Tian, X. Zhu, L. Weng and L. Wang, J. Mater. Chem., 2012, 22, 7791–7796.

[26] J. Kibsgaard, Y. Gorlin, Z. Chen and T. F. Jaramillo, J. Am.Chem. Soc., 2012, 134, 7758–7765.

[27] H. Li, J. Wang, M. Liu, H. Wang, P. Su, J. Wu and J. Li, Nano Research 2014, 7(7), 1007–1017

[28] X-L Sui, Z.-B. Wang, C.-Z. Li, J.-J. Zhang, L. Zhao, D.-M. Gu and S. Gu, J. Mater. Chem. A, 2015, 3, 840-846

[29] J.-J. Zhang, Z.-B. Wang, C. Li, L. Zhao, J. Liu , L.-M. Zhang and D.-M. Gu. Journal of Power Sources, 2015,289, 63-70

[30] S. Sharma and B.G. Pollet, Journal of Power Sources, 2012, 208, 96–119

[31]YS Yan, ZW Chen, LB Xu, WZ Li and M Waje. Nanotechnology 2006, 17(20), 5254-5259.

[32]L Niu, QH Li, FH Wei, X Chen and H Wang. J Electroanal Chem 2003, 544, 121-128.

[33]ZA Hu, LJ Ren, XJ Feng, YP Wang, YY Yang, J Shi, LP Mo and ZQ Lei. Electrochem Commun 2007, 9(1), 97-102.

[34] LZ Dai, YT Xu, XL Peng, HT Zeng and HH Wu. C.R. Chimie 2008, 11(1-2), 147-151

[35] G Wu, L Li, JH Li and BQ Xu. J Power Sources 2006, 155(2), 118-127.

[36]O.A. Khazova, A.A. Mikhaylova, E.K. Tusseeva, N.A. Mayorova, A.Y. Rychagov, Y.M. Volfkovich and A.V. Krestinin. Electrochim Acta 2011, 56(10), 3656-3665.

[37]C. Zhou, Z. Liu, Y. Yan, X. Du, Y.-W. Mai and S. Ringer. Nanoscale Res Lett 2011, 6, 1-6.

[38] S. Bhadra, D. Khastgir, N.K. Singha, J.H. Lee. Prog Polym Sci 2009, 34(8), 783-810

[39] E Antolini and ER Gonzalez. Appl Catal a-Gen 2009, 365(1), 1-19.

[40]Y. Chen, G.J. Zhang, J.A. Ma, Y.M. Zhou, Y.W. Tang and T.H. Lu. Int J Hydrogen Energ 2010, 35(19), 10109-10117.

[41]Z.P. Guo, D.M. Han, Z.W. Zhao, R. Zeng, Y.Z. Meng, D. Shu, H.K. Liu. J Power Sources 2008, 184(2), 361-369.

[42] E.T. Samulski and Y.C. Si. Chem Mater 2008, 20(21), 6792-6797.

[43] SI Woo, WC Choi, MK Jeon, JM Sohn, MR Kim and HJ Jeon. Adv Mater 2005, 17(4), 446-51

[44] L.C. Chen, C.L. Sun, M.C. Su, L.S. Hong, O. Chyan, C.Y. Hsu, K.H. Chen, T.F. Chang and L. Chang. Chem Mater 2005, 17(14), 3749-3753.

[45]Y.Y. Shao, J.H. Sui, G.P. Yin, and Y.Z. Gao. Appl Catal B-Environ 2008, 79(1-2), 89-99.

[46]C. Galeano, J. C. Meier, M. Soorholtz, H. Bongard, C. Baldizzone,K. J. J. Mayrhofer, and F. Schüth. ACS Catal. 2014, 4, 3856−3868

[47]P.L. Kuo and C.H. Hsu. ACS Appl Mater Inter 2011, 3(2), 115-118.

[48]B. Singh and E. Dempsey, RSC Adv., 2013, 3, 2279–2287

[49] R. Wang, D. C. Higgins, Md A. Hoque, D. Lee, F. Hassan and Z Chen. Sci Rep 2013, 3, 2431

[50] C. Zhang, L. Xu, N. Shan, T. Sun, J. Chen and Y.S Yan. ACS Catal. 2014, 4, 1926−1930

[51] C. Zhou, Z. Liu, X. Du, D.R.G. Mitchell, Y.W.Mai, Y.Yan and S.Ringer. Nanoscale Res Lett 2012, 7, 1-11.

[52] H. Meng, F. Xie, J. Chen, S. Sun and P. K. Shen. Nanoscale, 2011, 3, 5041-5048

[53] S. Ghosh and C. Retna Raj. J. Phys. Chem. C 2010, 114, 10843–10849

[54] L.-S. Zhang, X.-Q. Liang, W.-G. Song and Z.-Y. Wu. Phys. Chem. Chem. Phys., 2010, 12, 12055–12059

[55] W. Yang, Y. Wang, J. Li and X. Yang. Energy Environ. Sci., 2010, 3, 144–149

[56] E.Castillejos, P.-J. Debouttie` re, L. Roiban, A. Solhy, V. Martinez, Y. Kihn, O.Ersen, K.Philippot, B. Chaudret and P. Serp. Angew.Chem., Int. Ed. 2009, 48, 2529–2533.

[57] X. Pan and X. Bao. Acc. Chem. Res. 2011, 44, 553–562

[58] J Xiao, X. Pan, S. Guo, P. Ren and X. Bao. J. Am. Chem. Soc.2015, 1, 477-482

[59] H. Yue, Y. Zhao, S. Zhao, B. Wang, X. Ma, and J. Gong. Nat. Comm, 2013, 4, 2339

[60] DN Mastronarde. J Struct Biol 2005, 152(1), 36-51

[61] X. Du, Z.Z.Yu, A.Dasari, J.Ma, Y. Meng, and Y.W.Mai. Chem.Mater. 2006, 18, 5156-5158

[62] J.H. Bae, J.-H. Han and T. D. Chung. Phys. Chem. Chem. Phys. 2012, 14, 448−463.

[63] S. Wang, L. Kuai, Y. Huang, X. Yu, Y. Liu, W. Li, L. Chen, and B. Geng, Chem. Eur. J. 2013, 19, 240−248.

[64] M. Whitby and N. Quirke, Nat.Nanotechnol.2007, 2, 87-94

[65] H. G. Park and Y. Jung, Chem. Soc. Rev., 2014, 43, 565-576

[66] J. Wu, K. Gerstandt, H. Zhang, J. Liu and B. J. Hinds, Nat. Nanotechnol.2012, 7, 133-139

[67] F. Cheng, C. Yi, J. Liang, Z. Tao and J. Chen, J. Mater. Chem. 2009, 19, 4108−4116

Figure captions

Figure 1. X-ray diffraction pattern (a), SEM (b), bright-field TEM (c) and HRTEM micrograph (d) of TKCNT/Pt prepared after 72h. Inset of d is SAED of Pt nanorods.

Figure 2. TEM bright field micrographs of TKCNT/ Pt prepared at different time (a) 4h, (b) 12h, and (c) 36h.

Figure 3. (a) Cyclic voltammograms with scan rate of 50 mV/s and (b) Chronoamperograms at 0.7V for TKCNT/Pt, TNCNT/ Pt and CB/Pt; (c) Cyclic voltammograms with scan rate of 50 mV/s for the catalyst after the chronoamperogram tests in 1 M CH_3OH + 0.5 M H_2SO_4.

Figure 4. SEM micrographs (a) and TEM bright field micrographs (b-c) of TNCNT/Pt and (d)CB/Pt

Figure 5. Illustration of the cross section of CNT/Pt (a) and their 2D TEM image (b); Bright-field TEM (c) and Dark-field STEM (d) image of TKCNT/Pt.

Figure 6. Selected bright field images of TEM tilt series obtained by tilting the TKCNT/ Pt sample to different angles: +50°, +30°, 0°, -30° and -72°.

Figure 7. TEM tomography reconstructed images of TKCNT/Pt catalyst of the same sample in Figure 6 in longitudinal and transversal direction (inset).

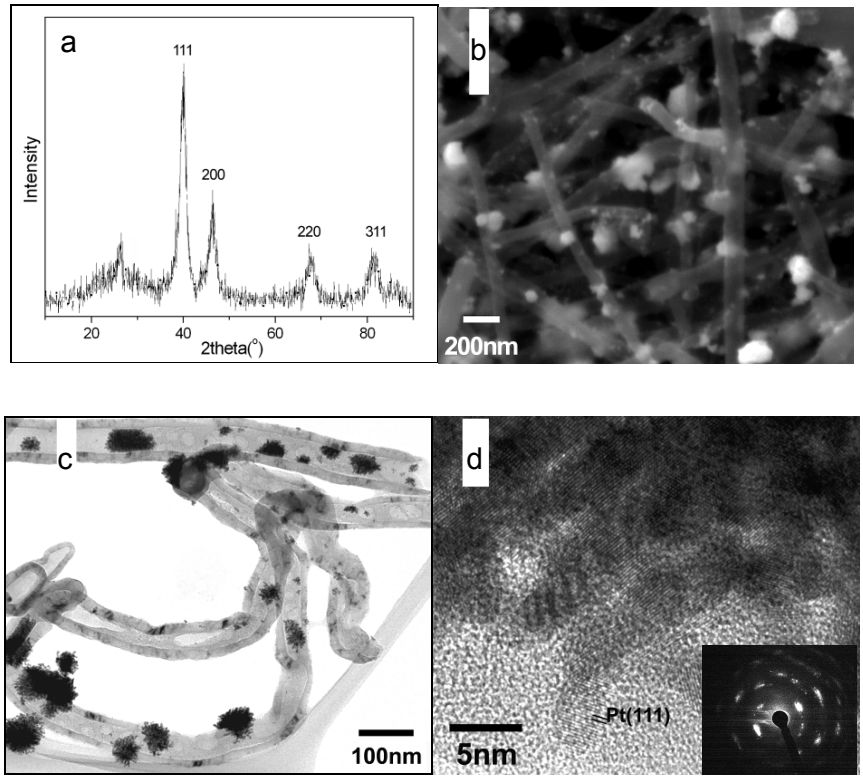

Figure 1

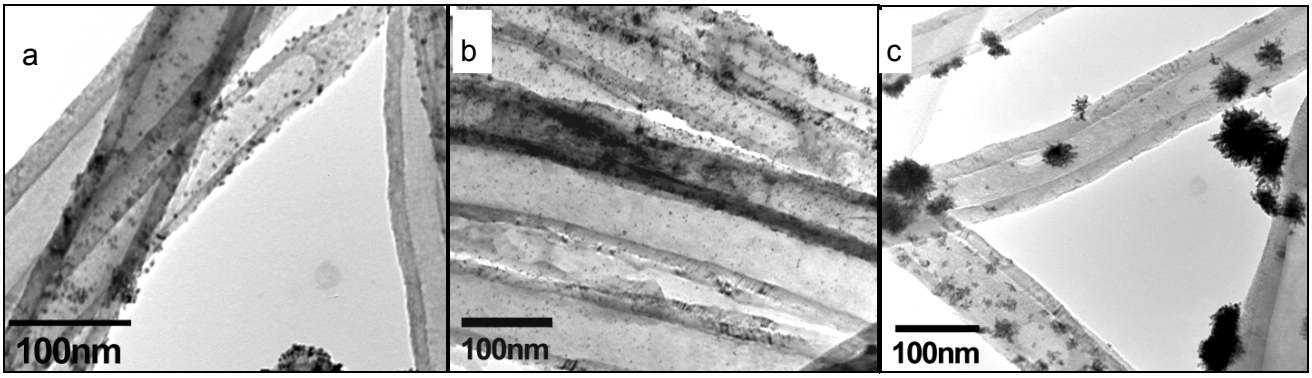

Figure 2

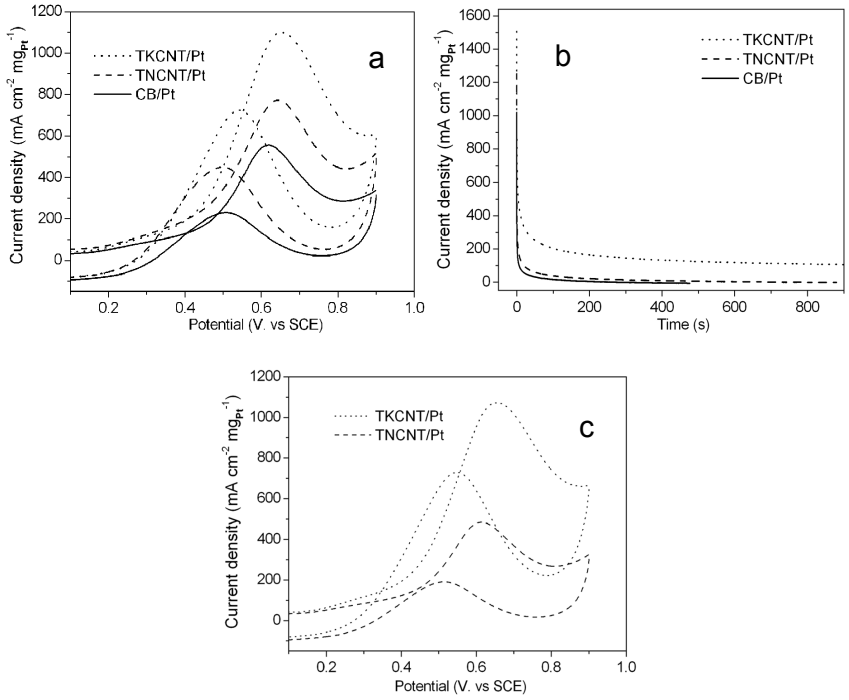

Figure 3

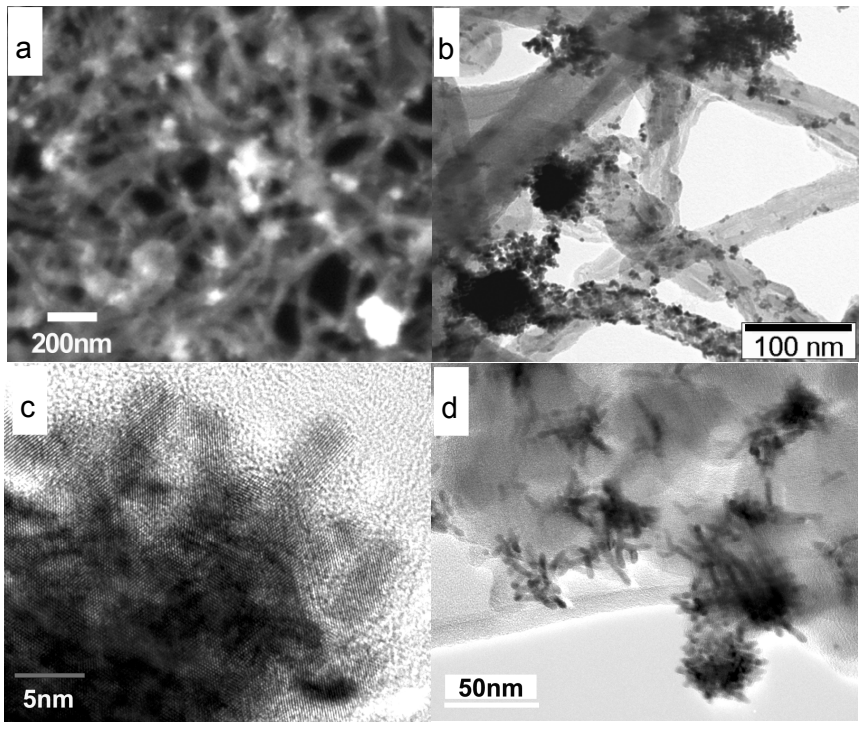

Figure 4

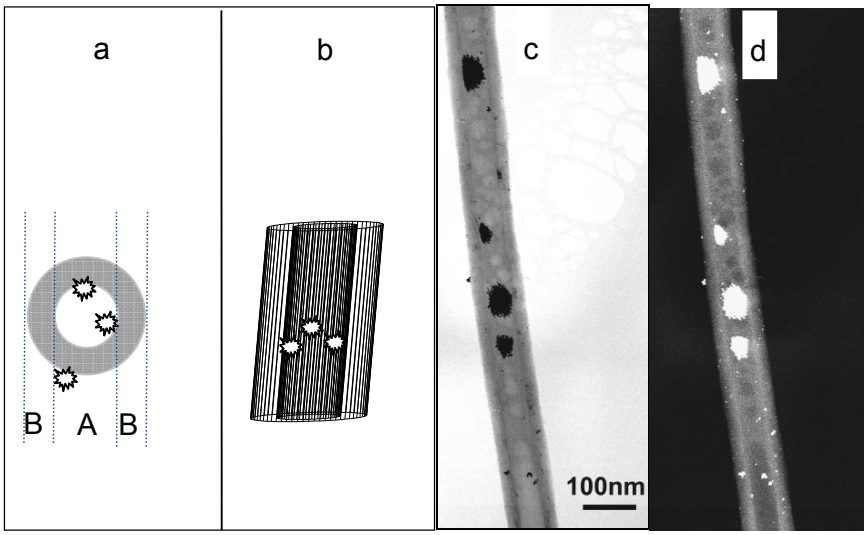

Figure 5

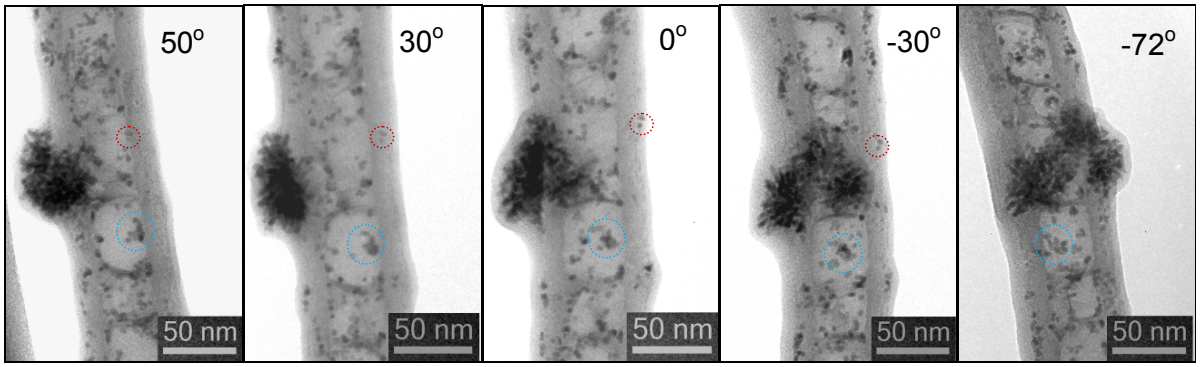

Figure 6

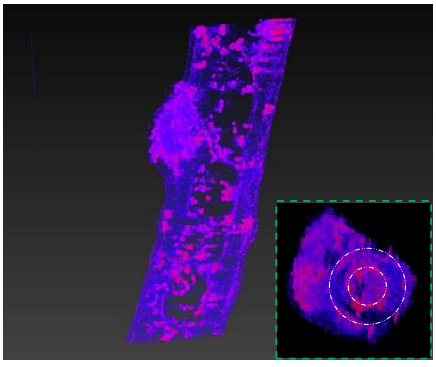

Figure 7